2020 American Control Conference
Denver, CO, USA, July 1-3, 2020

A Robust Energy and Emissions Conscious Cruise Controller for Connected Vehicles with Privacy Considerations

Chunan Huang[1], Xueru Zhang[2], Rasoul Salehi[1], Tulga Ersal[1] and Anna G. Stefanopoulou[1]

***Abstract*— While perturbation schemes for vehicle-to-vehicle (V2V) communications can address data privacy concerns, they can significantly compromise the performance of the speed controllers of connected automated vehicles (CAVs) if such controllers rely on the preview information available through V2V in car-following scenarios. This paper presents a robust predictive speed controller for a CAV when preview information is provided through a privacy-guaranteed V2V communication network. This is the first such controller that considers energy and emissions concurrently. The impact of privacy assurance in the communication data is studied, while inter-vehicular distance constraint is guaranteed to be satisfied through a robust design of the predictive controller using a robust control invariant set. The robust optimal speed controller is shown to reduce fuel consumption and emissions successfully while satisfying the constraints even in the presence of perturbations in the V2V communication. Results suggest a need for an integrated design procedure to achieve the best performance under a given level of privacy guarantee and emissions requirements.**

I. Introduction

Predictive speed control has shown high potential for improving the eco-driving performance of a connected automated vehicle (CAV) by adjusting the vehicle speed based on the upcoming traffic conditions [1]–[7]. In a car-following scenario, the preview information available about the leader vehicle can be leveraged by the CAV to estimate its future driving environment and optimize its speed trajectory to guarantee safety and improve the eco-driving performance. Although a majority of the literature focuses on fuel economy as the single eco-driving metric [2], [5], [8]–[10], previous studies have shown that it is crucial to simultaneously optimize emissions and fuel to avoid an increase in tailpipe emissions [11], [12].

The preview information about the leader vehicle can be obtained through velocity prediction [2], [8]–[10] and/or vehicle-to-vehicle (V2V) communication [2]. Either case presents a challenge for having an accurate preview. In the former case, it is difficult to predict the motion of the lead vehicle, as it needs to react to the movements of the other traffic participants, creating high uncertainty. In the latter case, even if the leader vehicle may know its future speed trajectory perfectly, perturbations may be applied to the information to be shared over V2V due to privacy concerns [13]. Hence, achieving a robust eco-driving performance while maintaining safety is an important challenge.

Some researchers have recognized this challenge and shown that preview inaccuracy can have disastrous impact on fuel-saving performance [2], [10]. They also developed a chance constrained model predictive controller (MPC) and a randomized MPC to reduce the risk of constraint violation and the fuel consumption at the same time. However, constraint violations still exist.

This material is based upon work supported by the National Science Foundation under Grant No. 1646019. The authors would like to thank Prof. Mingyan Liu from University of Michigan, Ann Arbor, for her help in explaining the work on differential privacy.

[1]C. Huang, R. Salehi, T. Ersal and A.G. Stefanopoulou are with the Department of Mechanical Engineering, University of Michigan, Ann Arbor, Michigan, 48109, USA. {huangchu,rsalehi,tersal,annastef}@umich.edu

[2]X. Zhang is with the Department of Electrical and Computer Engineering, University of Michigan, Ann Arbor, Michigan, 48109, USA. xueru@umich.edu

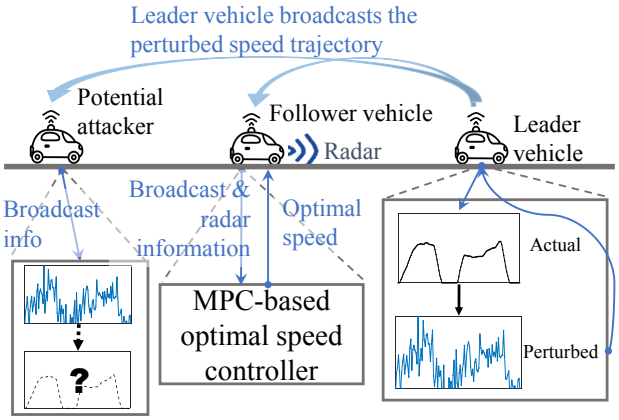

Fig. 1: Car-following traffic setup considered in this paper.

To resolve the constraint violation problem, provably-correct controllers have been designed when uncertainties exist in the speed preview. Controllers presented in [14], [15] generate car-following trajectories and satisfy minimum headway specifications, and controllers in [16]–[18] aim at avoiding collision with front vehicle. The main method used in the literature to synthesize the correct control variables is the calculation of a robust control invariant set. However, efforts typically focus only on the constraint satisfaction and only consider the vehicle kinematic performance. The only exception known to us is the work reported in [18], where the authors report 12% energy saving using their robust adaptive cruise controller compared with the non-optimized leader. However, to the best of our knowledge, there does not yet exist a fuel and emissions efficient controller that is robust to errors in preview information.

Recognizing this gap, in this work, we design and study an optimal speed controller that is robust to inaccuracies in leader vehicle velocity and is capable of concurrently optimizing fuel consumption and emissions. The formulation of the optimal speed controller is presented, and the effect of communication-imposed preview uncertainty on the performance of the controller is analyzed when disturbances are applied to shared information to guarantee privacy in a V2V network. Speed previews are generated simulating different levels of uncertainty and privacy guarantee through two methods, namely, adding zero-mean Gaussian noise and adopting the estimator-based method in [19].

II. Problem Setup

We consider a car-following scenario, where the ego-vehicle follows a leader vehicle and optimizes its velocity trajectory utilizing communicated information about the future motion of the leader [19].

A. Traffic scenario

The car-following traffic setup is shown in Fig. 1. The leader vehicle is assumed to have an on-board broadcast unit and to broadcast its perturbed speed for the next short future time horizon. Any other vehicle in the broadcast range

978-1-5386-8266-1/$31.00 ©2020 AACC

Authorized licensed use limited to: University of Michigan Library. Downloaded on September 26,2020 at 15:57:24 UTC from IEEE Xplore. Restrictions apply.

that has V2V capability has access to the broadcast [20]. The follower vehicle is assumed to be such a vehicle. It is further assumed that the follower is equipped with a front radar to measure the current inter-vehicular distance and velocity of the lead vehicle. All this information is fed into an MPC-based optimal speed controller on the follower vehicle, which utilizes the model of the follower vehicle to formulate an optimal control problem and generate a speed trajectory. The perturbation applied to the broadcast information aims at protecting the leader vehicle's privacy against the potential attacker, which is not the immediate follower. The potential attacker vehicle also has access to the broadcast information; however, it does not have access to the radar information that the follower vehicle has. Note that the perturbation mechanisms applied in this paper are not capable of protecting privacy of the leader vehicle against the follower vehicle.

B. Privacy-guaranteed perturbation methods

Two perturbations methods for private communication are considered.

One simple method to protect privacy is to add independent zero-mean Gaussian noise to the actual speed data, and this serves as the baseline perturbation method in this work. The disadvantage of this perturbation is that, as the information in consecutive broadcasts is highly correlated, an attacker can gather all the transmitted information and make an inference about the actual data.

The second perturbation method is the estimator-based method developed in [19]. In this method, the perturbed speed $\tilde{v}_\mathrm{l}(t)$ takes a convex combination of the actual speed $v_\mathrm{l}(t)$ and an estimation of true speed from the past information $\hat{v}_\mathrm{l}(t|t-1)$, and adds zero-mean Gaussian noise n to the combination:

$$\tilde{v}_\mathrm{l}(t) = (1-\alpha_t)\hat{v}_\mathrm{l}(t|t-1) + \alpha_t v_\mathrm{l}(t) + n, \tag{1}$$

α_t is the weight factor. $\hat{v}_\mathrm{l}(t|t-1)$ is the linear minimum mean square error (LMMSE) estimator given as $\hat{v}_\mathrm{l}(t|t-1) = \hat{\mu}_{t-1}\left(1-\hat{\rho}_{t-1}\frac{\hat{\sigma}^2_{t-1}}{\hat{\sigma}^2_{t-1}+\mathrm{Var}(n)}\right) + \hat{\rho}_{t-1}\frac{\hat{\sigma}^2_{t-1}}{\hat{\sigma}^2_{t-1}+\mathrm{Var}(n)}\tilde{v}_\mathrm{l}(t-1)$, where $\hat{\mu}_{t-1}$, $\hat{\rho}_{t-1}$ and $\hat{\sigma}^2_{t-1}$ are the estimated mean, variance and autocorrelation, respectively, which are calculated using all the perturbed speed in the history. Specifically, $\hat{\mu}_{t-1} = \frac{1}{t-1}\sum_{i=1}^{t-1}\tilde{v}_\mathrm{l}(i)$, $\hat{\sigma}^2_{t-1} = \max\{\frac{1}{t-2}\sum_{i=1}^{t-1}(\tilde{v}_\mathrm{l}(i)-\hat{\mu}_{t-1})^2 - \mathrm{Var}(n), 0\}$ and $\hat{\rho}_{t-1} = \frac{\sum_{i=1}^{t-2}(\tilde{v}_\mathrm{l}(i)-\hat{\mu}_{t-1})(\tilde{v}_\mathrm{l}(i+1)-\hat{\mu}_{t-1})}{\sum_{i=1}^{t-2}(\tilde{v}_\mathrm{l}(i)-\hat{\mu}_{t-1})^2}$.

By using the convex combination, less information about the actual speed is revealed because the history information (estimation) also contributes to the output. Therefore, noise n with smaller variance can be sufficient to achieve the same privacy guarantee compared with the baseline.

Two example trajectories of the randomly perturbed drive cycle using the baseline and estimator-based methods are shown in Fig. 2. The estimator-based method yields higher accuracy measured in root mean square error (RMSE), and is expected to yield better performance when it is used to provide preview to the optimal speed controller.

C. Modeling for the MPC

In the MPC, a vehicle model is adopted from the literature [12] to simulate the trajectory of the follower vehicle. Here we summarize this model for completeness.

The follower vehicle is assumed to be a point-mass system, with its discrete-time longitudinal dynamics modeled as:

$$\begin{bmatrix} p_\mathrm{f}(k+1) \\ v_\mathrm{f}(k+1) \end{bmatrix} = \begin{bmatrix} 1 & T_s \\ 0 & 1 \end{bmatrix} \begin{bmatrix} p_\mathrm{f}(k) \\ v_\mathrm{f}(k) \end{bmatrix} + \begin{bmatrix} 0.5T_s^2 \\ T_s \end{bmatrix} a_\mathrm{f}(k), \tag{2}$$

where p_f and v_f are the position and the speed of the follower vehicle, k is the step index, T_s is the sampling time, and

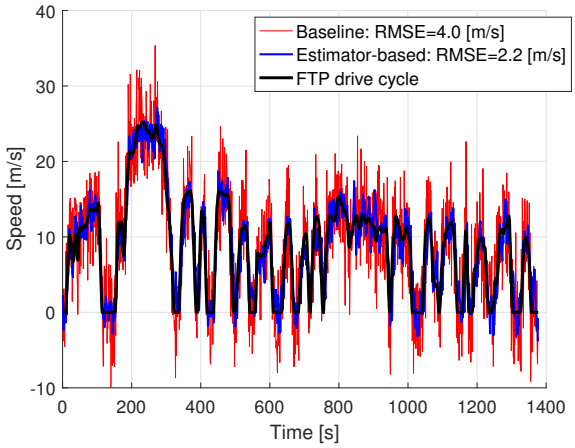

Fig. 2: Transmitted information perturbed by the baseline method and the estimator-based method under the same privacy guarantee.

$a_\mathrm{f}(k)$ is the acceleration of the follower vehicle. Using this vehicle dynamics model, as well as the gear shift and engine models adopted from [12], fuel rate $\dot{m}_\mathrm{Fuel}$, exhaust mass flow rate $\dot{m}_\mathrm{exh}$, engine raw NOx emissions $\dot{m}_\mathrm{NOx.Eng}$ and steady state turbine (TB) out temperature $T_\mathrm{TB.ss}$ are calculated using look-up tables mapped with vehicle speed v_f and acceleration a_f.

We consider the follower vehicle to be a diesel vehicle equipped with a selective catalytic reduction (SCR) aftertreatment system. For those vehicles, the tailpipe NOx emissions are determined by 1) the engine raw NOx emissions, and 2) the reduction efficiency η_AFT, which is largely affected by the catalyst temperature [21]. The turbine outlet gas temperature, T_TB, is the input temperature of the aftertreatment system, and the thermal dynamics of T_TB is modeled as [12]:

$$T_\mathrm{TB}(k+1) = T_\mathrm{TB}(k) + \frac{T_s}{\tau}(T_\mathrm{TB.ss}(k) - T_\mathrm{TB}(k)), \tag{3}$$

with τ being the time constant, which is a function of the exhaust mass flow rate $\dot{m}_\mathrm{exh}$. Both $\dot{m}_\mathrm{exh}$ and $T_\mathrm{TB.ss}$ are functions of the vehicle velocity v_f and acceleration a_f. Then, the tailpipe NOx emissions are obtained using

$$\dot{m}_\mathrm{NOx.TP} = \dot{m}_\mathrm{NOx.Eng}(1-\eta_\mathrm{AFT}), \tag{4}$$

where η_AFT and can be calculated using an aftertreatment thermal model and an efficiency model, with inputs T_TB, $\dot{m}_\mathrm{exh}$ and ambient temperature T_air:

$$\eta_\mathrm{AFT} = f_\eta(T_\mathrm{TB}, \dot{m}_\mathrm{exh}, T_\mathrm{air}). \tag{5}$$

D. Optimization objective function for the MPC

The goal of the MPC-based optimal speed controller is to reduce fuel consumption and tailpipe NOx emissions concurrently. Instead of penalizing the fuel and tailpipe NOx, which requires a complicated model, we set the objective function to be a weighted sum of squared acceleration and squared difference in turbine temperature from a predesigned threshold T_thr, when the previewed turbine temperature is lower than the threshold; i.e.,

$$\begin{aligned}\mathbf{J}(t) = \sum_{k=0}^{N_\mathrm{P}-1} \Big(& a_\mathrm{f}(k|t)^2 + \\ & w(T_\mathrm{TB}(k|t) - T_\mathrm{thr})^2 \cdot \mathscr{H}(T_\mathrm{thr} - T_\mathrm{TB}(k|t)) \Big),\end{aligned} \tag{6}$$

where $\mathscr{H}$ is the Heaviside step function, N_P is the prediction horizon, w is the equivalence factor to balance fuel consumption and emissions, and the notation $\bullet(k|t)$ refers to the

Authorized licensed use limited to: University of Michigan Library. Downloaded on September 26,2020 at 15:57:24 UTC from IEEE Xplore. Restrictions apply.

predicted value of the variable $\bullet$ at time step $(t+k)$ given the information at time step t. The term $a_{\mathrm{f}}(k|t)$ in the objective function (6) represents fuel consumption, since reducing large acceleration and deceleration is shown to effectively reduce the vehicle fuel consumption [3], [12]. Similarly, increasing the turbine temperature has been shown experimentally as an effective method to increase the temperature of the SCR system on the downstream [22]. This formulation aims to strike a balance between reducing acceleration and maintaining turbine temperature, and it has been shown that this formulation is able to balance fuel consumption and tailpipe NOx emissions [23].

III. Predictive Speed Controller Design

The MPC-based speed controller is taking an iterative approach, deciding at every time step the optimal speed trajectory for the next horizon while satisfying pre-defined state and input constraints. In this paper, we consider constraints on maximum/minimum acceleration and velocity:

$$a_{\mathrm{f}} \in \mathscr{U} = [-\underline{a_{\mathrm{f}}}, \overline{a_{\mathrm{f}}}], \tag{7}$$

$$\underline{v} \leq v_{\mathrm{f}}(k+1|t) \leq \overline{v}, \tag{8}$$

and following distance constraints based on a minimum and maximum time headway (τ_1, τ_2) policy [24] with (d_{c1}, d_{c2}) as the standstill distances:

$$p_{\mathrm{l}}(k+t+1) - p_{\mathrm{f}}(k+1|t) \geq \tau_1 v_{\mathrm{f}}(k+1|t) + d_{c1}, \tag{9a}$$

$$p_{\mathrm{l}}(k+t+1) - p_{\mathrm{f}}(k+1|t) \leq \tau_2 v_{\mathrm{f}}(k+1|t) + d_{c2}, \tag{9b}$$

where p_{l} denotes the position of the leader vehicle.

A. Original MPC

We consider the following optimal control problem as the original MPC, which is adopted from a similar formulation in [23]:

$$\min_{U,\varepsilon} \quad \mathbf{J}(t) + c_\varepsilon \varepsilon, \tag{10a}$$

$$\text{subject to} \quad a_{\mathrm{f}}(k|t) \in \mathscr{U} \tag{10b}$$

$$\underline{v} \leq v_{\mathrm{f}}(k+1|t) \leq \overline{v} \tag{10c}$$

$$\hat{p}_{\mathrm{l}}(k+t+1) - p_{\mathrm{f}}(k+1|t) \geq \tau_1 v_{\mathrm{f}}(k+1|t) + d_{c1} - \varepsilon \tag{10d}$$

$$\hat{p}_{\mathrm{l}}(k+t+1) - p_{\mathrm{f}}(k+1|t) \leq \tau_2 v_{\mathrm{f}}(k+1|t) + d_{c2} + \varepsilon \tag{10e}$$

$$\varepsilon \geq 0 \tag{10f}$$

$$a_{\mathrm{f}}(0|t) \in \mathscr{U} \tag{10g}$$

$$\text{Eqns. (2) and (3).} \tag{10h}$$

for $k = 0, 1, ..., N_{\mathrm{P}} - 1$.

$U = \begin{bmatrix} a_{\mathrm{f}}(0|t) & a_{\mathrm{f}}(1|t) & \cdots & a_{\mathrm{f}}\big((N_{\mathrm{P}}-1)|t\big) \end{bmatrix}^T$ and ε are the decision variables of the optimal control problem. $\hat{p}_{\mathrm{l}}$ is the prediction of the position of the leader (p_{l}) calculated using the speed preview, and we assume the leader follows the same dynamics as (2). (10b) to (10e) are essentially the constraints (7), (8), (9a) and (9b) when the prediction of position instead of the actual position is available.

Different from [23], a slack variable ε is used here to change a hard (distance) constraint into a soft one and penalize the constraint violation in the cost function with a scaling factor c_ε. A large value for c_ε is chosen. Introducing ε avoids feasibility problems that may happen when hard constraints are used. Note that a feasible solution to this optimal control problem can always be found, but feasibility does not guarantee the satisfaction of the constraints (9a) and (9b) as $\hat{p}_{\mathrm{l}}$ may not be equal to p_{l}.

After solving for the optimal U, only $U(1) = a_{\mathrm{f}}(0|t)$ is applied to the follower vehicle, and then the MPC is solved again with updated states. For the original MPC, we do not impose any additional constraint on $a_{\mathrm{f}}(0|t)$ except the pre-defined constraint (7).

B. Robust MPC

Because of the potential existence of collisions and headway constraint violations due to the inaccurate speed preview, using the original MPC formulation above may lead to violation of the speed or position constraints. To avoid possible violation of the distance constraints in the executed follower vehicle profile, we first use a feedback controller to compute the safe action set $\mathscr{U}^*(t)$ at time t:

$$\mathscr{U}^*(t) = \mathscr{U}^*(d(t), v_{\mathrm{f}}(t), v_{\mathrm{l}}(t)). \tag{11}$$

The set $\mathscr{U}^*(t)$ denotes the set of all admissible accelerations $a_{\mathrm{f}}(0|t)$ at time t that ensure existence of a trajectory for the follower vehicle, which always satisfies velocity and headway constraints (8), (9a) and (9b) for an uncertain (but bounded) leader vehicle acceleration trajectory. More details are provided later in this section.

After obtaining $\mathscr{U}^*(t)$ from the feedback controller, we add this new constraint on $a_{\mathrm{f}}(0|t)$ to the original MPC (10).

$$\min_{U,\varepsilon} \quad \mathbf{J}(t) + c_\varepsilon \varepsilon, \tag{12a}$$

$$\text{subject to} \quad \text{Eqns. (10b) - (10f)} \tag{12b}$$

$$a_{\mathrm{f}}(0|t) \in \mathscr{U}^*(d(0|t), v_{\mathrm{f}}(0|t), v_{\mathrm{l}}(0|t)) \tag{12c}$$

$$\text{Eqns. (2) and (3).} \tag{12d}$$

The new MPC formulation in (12) has the following features: 1) Keeping ε as in the original MPC formulation ensures persistent feasibility. 2) Using (12c) ensures that the speed profile of the follower at time t is robust to uncertainty in the leader speed preview, as guaranteed by (18). 3) Satisfaction of the distance constraints (10d) and (10e) with $\varepsilon = 0$ is not guaranteed throughout the horizon.

C. Calculation of the safe action set $\mathscr{U}^*$

Here we present the steps to calculate $\mathscr{U}^*$, the safe action set, from a robust control invariant set inside an admissible set $\mathscr{X}$. We start with the definition of an invariant set.

Consider the leader-follower system with states $x = \begin{bmatrix} d & v_{\mathrm{f}} & v_{\mathrm{l}} \end{bmatrix}^T$, and system dynamics represented as:

$$\begin{aligned} &x(k+1) = Ax(k) + Ba_{\mathrm{f}}(k) + Ga_{\mathrm{l}}(k), \\ &A = \begin{bmatrix} 1 & -T_s & T_s \\ 0 & 1 & 0 \\ 0 & 0 & 1 \end{bmatrix}, B = \begin{bmatrix} -T_s^2/2 \\ T_s \\ 0 \end{bmatrix}, G = \begin{bmatrix} T_s^2/2 \\ 0 \\ T_s \end{bmatrix}, \end{aligned} \tag{13}$$

since we assume the leader follows the same dynamics as (2). In the above equations, v_{l} and a_{l} represent the velocity and acceleration of the leader vehicle. We define the set of admissible states as:

$$\mathscr{X} = \{x \in \mathbb{R}^3 : d_{c1} + \tau_1 v_{\mathrm{f}} \leq d \leq d_{c2} + \tau_2 v_{\mathrm{f}}, 0 \leq v_{\mathrm{f}}, v_{\mathrm{l}} \leq \overline{v}\}. \tag{14}$$

The set Ω^* is a robust control invariant set of $\mathscr{X}$ if:

$$\forall x(k) \in \Omega^*, \exists a_{\mathrm{f}}(k) \in \mathscr{U}, s.t.\ x(k+1) \in \Omega^*, \forall a_{\mathrm{l}}(k) \in \mathscr{W}\big(x(k)\big), \tag{15}$$

where $\mathscr{W}$ is the set of possible disturbances (leader accelerations) defined as:

$$\mathscr{W}\big(x(k)\big) \stackrel{\text{def}}{=} \{a_{\mathrm{l}}(k) \in \mathbb{R}^1 : \underline{a_{\mathrm{l}}} \leq a_{\mathrm{l}}(k) \leq \overline{a_{\mathrm{l}}}, x_{\mathrm{l}}(k+1) \in \mathscr{X}\}. \tag{16}$$

To find Ω^*, we introduce the $Pre(\mathscr{X})$ operator, which gives the one-step (backward) robustly controllable set of set $\mathscr{X}$:

$$\begin{aligned} Pre(\mathscr{X}) \stackrel{\text{def}}{=} \{&x(k) \in \mathbb{R}^3 : \exists a_{\mathrm{f}}(k) \in \mathscr{U}, s.t. \\ &x(k+1) \in \mathscr{X}, \forall a_{\mathrm{l}}(k) \in \mathscr{W}\big(x(k)\big)\}. \end{aligned} \tag{17}$$

Calculation of Ω^* relies on finding the fixed point for the $Pre(\mathscr{X})$ operator using the following iterative algorithm:

Authorized licensed use limited to: University of Michigan Library. Downloaded on September 26,2020 at 15:57:24 UTC from IEEE Xplore. Restrictions apply.

Algorithm 1 Calculation of Ω^*

Initialize $\Omega_0 = \mathscr{X}$

While $\Omega_k \not\subseteq \Omega_{k+1}$

$\Omega_{k+1} = \mathscr{X} \cap Pre(\Omega_k)$

End

Return $\Omega^* = \Omega_{k+1}$

TABLE I: Parameters for the example in Sec. III-E

Parameter	Description	Range
$\underline{v}, \overline{v}$	min,max speed	$0, 30$ [m/s]
$\underline{a_f}, \overline{a_f}$	min,max follower acceleration	$-6, 6$ [m/s^2]
$\underline{a_l}, \overline{a_l}$	min,max leader acceleration	$-3, 3$ [m/s^2]
τ_1, τ_2	min,max time headway	$1, 4$ [s]
d_{c1}, d_{c2}	min,max standstill distance	$0, 10$ [m]
T_s	sampling time	1 [s]

Calculation of $Pre(\Omega_k)$ from Ω_k is done using the Multi-Parametric Toolbox [25] in Matlab and following the steps proposed in [26].

The range of input that allows the state to remain inside Ω^*, $\mathscr{U}^*(x)$, is calculated by:

$$\mathscr{U}^*(x) \stackrel{\text{def}}{=} \{a_f \in \mathscr{U} : Ax + Ba_f + Ga_l \in \Omega^*, \forall a_l \in \mathscr{W}(x)\}, \quad (18)$$

with current states $x = [d \quad v_f \quad v_l]^T \in \Omega^*$. Since Ω^* is a union of polyhedra, the above set $\mathscr{U}^*(x)$ of a_f is a union of intervals, and the end points can be solved using linear programming to find the maximum/minimum a_f that satisfies (18).

D. Numerical problems in calculation of robust control invariant set

All the sets above are convex polyhedra represented by linear inequalities, or non-convex polyhedra represented by unions of convex polyhedra. Although this algorithm works for a variety of systems, the algorithm may not terminate due to numerical issues, and manual termination may lead to an over-approximation, which is no more robust control invariant [14]. A way to avoid this issue and always produce a robust control invariant set is to use the Inside-out algorithm [14], [27]. The key is to first find a small robust control invariant set $\tilde{\Omega}$ contained in Ω_0, and then expand into a larger invariant set Ω^* by calculating its one-step robustly controllable set. The union of a small robust control invariant set and its one-step robustly controllable set is still robustly control invariant, since there exist a control input that will bring any point in this union back into the small robust control invariant set.

E. Numerical example

As a numerical example, we consider the speed and acceleration constraints in (10) to have the parameters in Table I. Then, the set of admissible states (14) is set up to be:

$$\mathscr{X} = \{x \in \mathbb{R}^3 : v_f \le d \le 10 + 4v_f, 0 \le v_f, v_l \le 30\}. \quad (19)$$

After performing the Inside-out algorithm, Ω^* used in this paper is a union of polyhedra, as shown in Fig. 3.

IV. Results

Four scenarios are tested to evaluate the different eco-following controller frameworks:

S1. OMPC-base: Original MPC with speed preview generated using the baseline perturbation

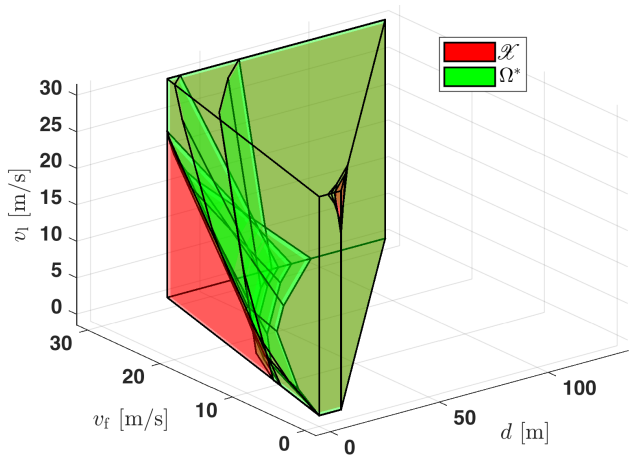

Fig. 3: The set $\mathscr{X}$ of admissible states and the robust control invariant set Ω^* calculated through the Inside-out algorithm.

TABLE II: Root Mean Square Error of perturbed drive cycle (m/s) with baseline perturbation and estimator-based at different privacy levels.

Privacy Level (PL)	Baseline	Estimator-based
1	2.0	1.5
2	4.0	2.1
3	6.0	2.9
4	8.0	3.7

S2. OMPC-est: Original speed controller with speed preview generated using the estimator-based perturbation

S3. RMPC-base: Robust speed controller with speed preview generated using the baseline perturbation

S4. RMPC-est: Robust speed controller with speed preview generated using the estimator-based perturbation

Each scenario is tested with the leader vehicle's broadcast speed profile perturbed to privacy guarantee levels of $[1, 2, 3, 4]$, associated with cases where baseline perturbation is using Gaussian noise with RMSE $[2, 4, 6, 8]$ m/s. The RMS estimation errors of the leader vehicle speed using the perturbed data are shown in Table II with the estimator-based method showing better accuracy than the baseline method under the same privacy level [19]. Similar to the previous work, the follower vehicle speed is optimized for the last 880s (the second bag of FTP drive cycle) and the equivalence factor w is swept from 0 to 0.5 with a step size of 0.1. A detailed aftertreatment model and emission model are utilized to evaluate η_{AFT} in (5), the efficiency of the aftertreatment, and $\dot{m}_{\text{NOx.TP}}$, the tailpipe emissions in (4) [12].

A. Robust collision avoidance

The total time that the headway minimum or maximum distance constraints are violated is shown in Fig. 4 for different test scenarios and privacy levels. As shown, with the original MPC formulation the headway constraint violations happen even when the estimator-based perturbation method with small preview errors is used. However, using the robust MPC design, the controller is persistently feasible and can always satisfy both the pre-defined minimum and maximum headway constraints as the time trace in Fig. 5 shows, independent of the perturbation size and privacy level. Fig. 4 also indicates that although the speed preview is more accurate when the estimator-based perturbation method is used, the time for constraint violation is longer compared to the baseline data perturbation method. Thus, this observation further motivates the use of a provably robust speed controller to guarantee constraint satisfaction.

Authorized licensed use limited to: University of Michigan Library. Downloaded on September 26,2020 at 15:57:24 UTC from IEEE Xplore. Restrictions apply.

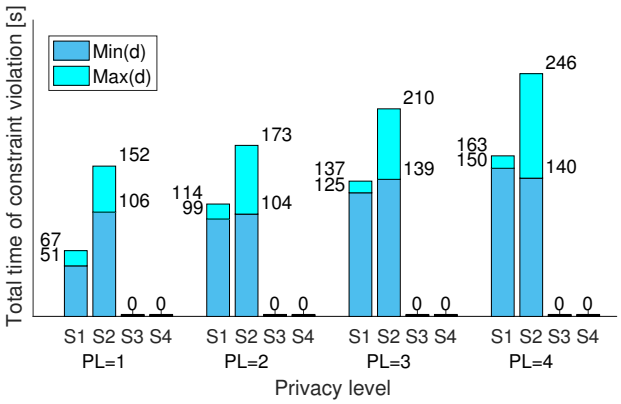

Fig. 4: The total time of minimum and maximum distance constraint violations for various levels of privacy, perturbation method and speed controller. The controller parameters are the same and the equivalence factor is $w = 0.1$. S1-S4 refer to the scenarios as listed at the beginning of Sec. IV.

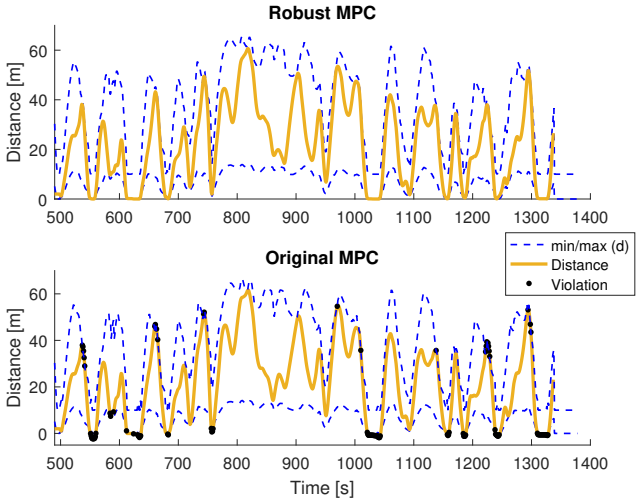

Fig. 5: Traces of following distance and constraints with privacy level 2. Perturbed with baseline method, RMSE $= 4$ and equivalence factor $w = 0.1$.

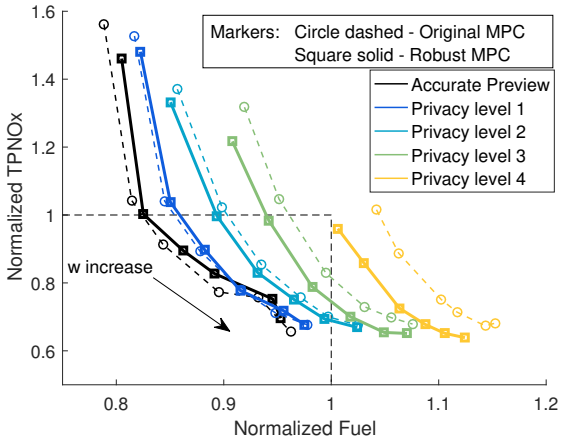

Fig. 6: Comparison of original vs. robust speed controller with baseline perturbation. The plotted accumulative mass of fuel and tailpipe NOx are normalized with the corresponding values when the vehicle is driven with the nominal FTP speed trajectory, i.e., the same drive cycle as the leader.

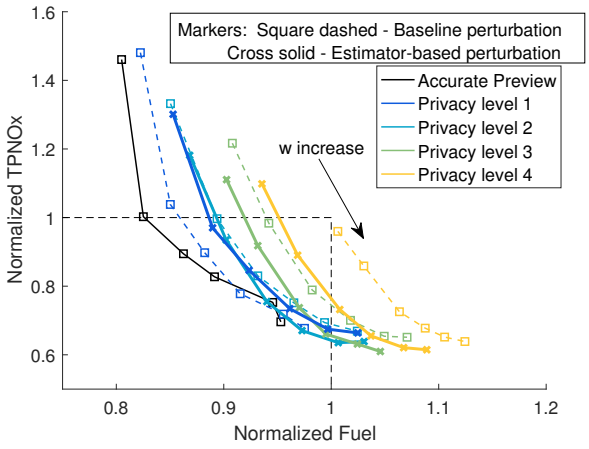

Fig. 7: Impact of perturbation method on fuel-NOx performance calculated using the robust speed controller.

B. *Fuel consumption and tailpipe emissions*

The degradation of the controller performance due to increased uncertainty in the speed preview is shown in Fig. 6. The results show a monotonic increase in the vehicle fuel consumption and tailpipe emissions when standard deviation of the preview error increases due to increasing privacy levels. The energy and emission conscious predictive controller with the robust formulation can reduce both fuel and tailpipe emissions with up to 4% fuel saving even using a data privacy as high as level 3, which means the standard deviation of the Gaussian error is more than $1/3$ of the actual speed (with 6 m/s RMSE). This demonstrates the robustness of the presented controller formulation. Fig. 6 also shows how the fuel-NOx performance improves when the safe robust MPC is used, which reduces the absolute value of the input accelerations. With the original MPC, due to the large errors in the speed preview, the follower vehicle observes the leader as an aggressive driver; thus, it reacts aggressively to the leader vehicle maneuvers to keep the headway distance. This behavior results in a more energy-demanding trajectory and sacrifices the performance on fuel and emissions.

The effect of perturbation method on fuel-NOx performance of the robust speed controller is shown in Fig. 7. Since the estimator-based perturbation method provides more accurate speed information compared to the baseline perturbation method, the speed controller performance improves and lower fuel consumption can be achieved at for a given tailpipe emissions level. Therefore, with the robust fuel and emissions conscious MPC formulation and estimator-based perturbation method in the V2V communication, the follower vehicle improves the fuel consumption without increasing the tailpipe emissions even with a privacy level as high as 4.

C. *Potentials with an integrated design procedure*

1) Perturbation mechanism: Baseline perturbation with privacy level 1 provides a better input for the robust speed controller than the particular design considered for the estimator-based perturbation, which has the same privacy guarantee and less RMSE. Thus, it remains as an open question what measure should be used to evaluate the quality of preview. Theoretically, there should exist a well-tuned perturbation mechanism that performs no worse than the baseline, since the baseline is the special case of selecting the share on the speed estimation to be 0 in the convex combination in Sec. II-B. Further, as mentioned in Sec. II-B, better estimation methods may be used to improve estimation accuracy without adding privacy leakage. Thus, this expresses the need for future studies to consider the application of the perturbed information in the design process of the perturbation method to find a design that achieves best controller performance (e.g., fuel-NOx trade-off) under the same privacy guarantee.

Authorized licensed use limited to: University of Michigan Library. Downloaded on September 26,2020 at 15:57:24 UTC from IEEE Xplore. Restrictions apply.

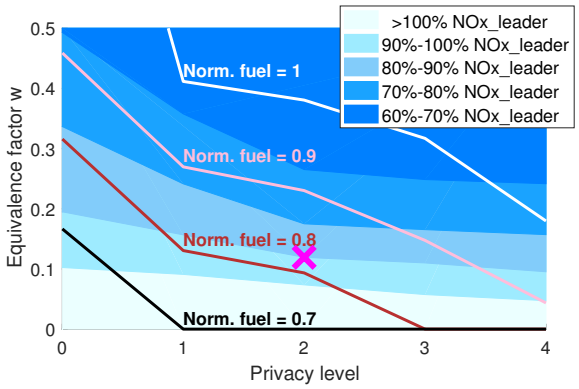

Fig. 8: Fuel consumption and NOx emissions varying with equivalence factor w under different privacy levels using the estimator-based perturbation method. Cross marker shows the most fuel efficient choice of w with 10% emissions improvement. Privacy level 0 represents the case with accurate preview.

2) Speed controller parameterization: If preview uncertainty is known ahead of time, then it would be possible to design the equivalence factor based on the level of uncertainty for largest fuel efficiency and maintain certain level of NOx emissions. Fuel and emissions performances vary with privacy level and choice of equivalence factor w as shown in Fig. 8. This figure also provides a map-based approach for w selection under fuel consumption or emissions constraints. For instance, if privacy level is required to be 2 and 10% improvement is desired in NOx emissions compared with following the leader trajectory exactly, choosing $w \approx 0.13$ as shown by the cross marker in the figure leads to the largest fuel efficiency improvement (between 10%-20%). If the level of uncertainty is not known beforehand, it may be adapted as better knowledge is obtained about the uncertainty while the controller is running.

V. Conclusions

An application of predictive speed planning for CAVs in a car-following scenario is studied considering the uncertainty in preview information due to privacy considerations. A robust energy and emissions-efficient optimal speed controller is developed for a diesel-powered ego vehicle and is shown in simulation to guarantee constraint satisfaction for inter-vehicular distance under preview error. Simulations also show the effectiveness of this robust controller to improve fuel and emissions performances with large preview error. Further improvements are achieved when an estimator-based privacy-guaranteeing perturbation method is used. Due to the different behaviors of fuel and emissions when privacy and thus uncertainty level increases, as well as the observation that the perturbation method that has a smaller root mean square error does not always lead to a better controller performance, results suggest inclusion of the privacy level into the design process for preview perturbation and the optimal speed controller to achieve better controller performance.

References

[1] B. Asadi and A. Vahidi, "Predictive cruise control: Utilizing upcoming traffic signal information for improving fuel economy and reducing trip time," *IEEE Transactions on Control Systems Technology*, vol. 19, no. 3, pp. 707–714, 2010.

[2] D. Moser, R. Schmied, H. Waschl, and L. del Re, "Flexible spacing adaptive cruise control using stochastic model predictive control," *IEEE Transactions on Control Systems Technology*, vol. 26, no. 1, pp. 114–127, 2018.

[3] N. Prakash, G. Cimini, A. G. Stefanopoulou, and M. J. Brusstar, "Assessing fuel economy from automated driving: Influence of preview and velocity constraints," in *2016 Dynamic Systems and Control Conference*, 2017.

[4] D. Lang, T. Stanger, and L. del Re, "Opportunities on fuel economy utilizing V2V based drive systems," *SAE Technical Paper 2013-01-0985*, 2013.

[5] T. Stanger and L. del Re, "A model predictive cooperative adaptive cruise control approach," in *American Control Conference*, 2013, pp. 1374–1379.

[6] F. Mensing, E. Bideaux, R. Trigui, and H. Tattegrain, "Trajectory optimization for eco-driving taking into account traffic constraints," *Transportation Research Part D: Transport and Environment*, vol. 18, pp. 55–61, 2013.

[7] V. Turri, B. Besselink, and K. H. Johansson, "Cooperative look-ahead control for fuel-efficient and safe heavy-duty vehicle platooning," *IEEE Transactions on Control Systems Technology*, vol. 25, no. 1, pp. 12–28, 2017.

[8] S. Li, K. Li, R. Rajamani, and J. Wang, "Model predictive multi-objective vehicular adaptive cruise control," *IEEE Transactions on Control Systems Technology*, vol. 19, no. 3, pp. 556–566, 2011.

[9] C. Huang, R. Salehi, T. Ersal, and A. G. Stefanopoulou, "Optimal speed planning using limited preview for connected vehicles with diesel engines," in *14th International Symposium on Advanced Vehicle Control*, 2018.

[10] C. R. He and G. Orosz, "Saving fuel using wireless vehicle-to-vehicle communication," in *2017 American Control Conference*, 2017, pp. 4946–4951.

[11] R. Schmied, H. Waschl, R. Quirynen, M. Diehl, and L. del Re, "Nonlinear MPC for emission efficient cooperative adaptive cruise control," *IFAC-papersonline*, vol. 48, no. 23, pp. 160–165, 2015.

[12] C. Huang, R. Salehi, and A. G. Stefanopoulou, "Intelligent cruise control of diesel powered vehicles addressing the fuel consumption versus emissions trade-off," in *2018 American Control Conference*, 2018, pp. 840–845.

[13] "Danger ahead: The governments plan for vehicle-to-vehicle communication threatens privacy, security, and common sense," https://www.eff.org/deeplinks/2017/05/danger-ahead-governments-plan-vehicle-vehicle-communication-threatens-privacy, Posted: 2017-05-08.

[14] P. Nilsson, O. Hussien, A. Balkan, Y. Chen, A. D. Ames, J. W. Grizzle, N. Ozay, H. Peng, and P. Tabuada, "Correct-by-construction adaptive cruise control: Two approaches," *IEEE Transactions on Control Systems Technology*, vol. 24, no. 4, pp. 1294–1307, 2016.

[15] C. He and G. Orosz, "Safety guaranteed connected cruise control," in *IEEE International Conference on Intelligent Transportation Systems*, 2018, pp. 549–554.

[16] S. Lefèvre, A. Carvalho, and F. Borrelli, "A learning-based framework for velocity control in autonomous driving," *IEEE Transactions on Automation Science and Engineering*, vol. 13, no. 1, pp. 32–42, 2016.

[17] C. Massera Filho, M. H. Terra, and D. F. Wolf, "Safe optimization of highway traffic with robust model predictive control-based cooperative adaptive cruise control," *IEEE Transactions on Intelligent Transportation Systems*, vol. 18, no. 11, pp. 3193–3203, 2017.

[18] Y. Kim, J. Guanetti, and F. Borrelli, "Robust eco adaptive cruise control for cooperative vehicles," in *2019 European Control Conference*, 2019, pp. 1214–1219.

[19] X. Zhang, C. Huang, M. Liu, A. G. Stefanopoulou, and E. Tulga, "Predictive cruise control with private vehicle-to-vehicle communication for improving fuel consumption and emissions," *IEEE Communications Magazine*, vol. 57, no. 10, pp. 91–97, 2019.

[20] J. B. Kenney, "Dedicated short-range communications (DSRC) standards in the United States," *Proceedings of the IEEE*, vol. 99, no. 7, pp. 1162–1182, 2011.

[21] G. Cavataio, H.-W. Jen, J. R. Warner, J. W. Girard, J. Y. Kim, and C. K. Lambert, "Enhanced durability of a Cu/zeolite based SCR catalyst," *SAE International Journal of Fuels and Lubricants*, vol. 1, no. 1, pp. 477–487, 2009.

[22] H. Wassen, J. Dahl, and A. Idelchi, "Holistic diesel engine and exhaust after-treatment model predictive control," in *2019 IFAC International Symposium on Advances in Automotive Control*, 2019, pp. 347–352.

[23] C. Huang, R. Salehi, E. Tulga, and A. G. Stefanopoulou, "An energy and emissions conscious adaptive cruise controller for a connected automated diesel truck," *Vehicle System Dynamics*, 2020, in press, doi:10.1080/00423114.2020.1740283.

[24] D. Swaroop and K. Rajagopal, "A review of constant time headway policy for automatic vehicle following," in *2001 IEEE Intelligent Transportation Systems Conference*, 2001, pp. 65–69.

[25] M. Herceg, M. Kvasnica, C. N. Jones, and M. Morari, "Multi-parametric toolbox 3.0," in *2013 European Control Conference*, 2013, pp. 502–510.

[26] S. V. Rakovic, E. C. Kerrigan, and D. Q. Mayne, "Reachability computations for constrained discrete-time systems with state-and input-dependent disturbances," in *2003 IEEE International Conference on Decision and Control*, vol. 4, 2003, pp. 3905–3910.

[27] E. De Santis, M. D. Di Benedetto, and L. Berardi, "Computation of maximal safe sets for switching systems," *IEEE Transactions on Automatic Control*, vol. 49, no. 2, pp. 184–195, 2004.

Authorized licensed use limited to: University of Michigan Library. Downloaded on September 26,2020 at 15:57:24 UTC from IEEE Xplore. Restrictions apply.